(Received 26 May 2026, Accepted 17 June 2026, Scheduled 7 July 2026)

An Improved Black-Winged Kite Algorithm with Harmonic Compensation for PMSM Parameter Identification

Yang Zhang, Shaoziyi Wu, Gao Tang, Jiahao Zhang, Wancheng Xie, and Qianghui Xiao*

Hunan University of Technology, Zhuzhou 412007, China

ABSTRACT: To improve the accuracy and stability of parameter identification for permanent magnet synchronous motor (PMSM) drives, which are affected by the dead-time nonlinearity of the voltage source inverter (VSI), this study presents an enhanced Black-winged Kite Algorithm (BKA) integrated with 5th- and 7th-order harmonic voltage compensation. Initially, harmonic compensation targeting the 5th and 7th voltage components is introduced to suppress the detrimental influence of the VSI dead time on both identification precision and operational stability. Subsequently, a Good Point Set-based initialization approach is adopted to distribute the initial population more evenly across the search domain, which contributes to improved population diversity and algorithmic consistency. In addition, the Thinking Innovation Strategy (TIS) is embedded into the exploration stage of the black-winged kite algorithm to strengthen its global optimization capability. Experimental investigations across different operating scenarios demonstrated that the proposed method achieved superior effectiveness and improved performance.

1. INTRODUCTION

Driven by the rapid advancement of electric vehicles, aerospace technologies, and robotic systems, permanent magnet synchronous motors (PMSMs) have been widely adopted as core actuators because of their outstanding characteristics, including high power density, broad speed control capability, and excellent dynamic performance [1, 2]. However, the control performance of PMSMs depends heavily on the accuracy of the motor mathematical model parameters [3–6]. During actual operation, the electrical parameters of PMSM are not constant. The stator resistance varies with ambient temperature, and the stator inductance exhibits nonlinear characteristics owing to the magnetic saturation effect. The flux linkage is affected by temperature and demagnetizing current [7]. In addition, the dead-time effect of the voltage source inverter (VSI) further degrades the accuracy and stability of parameter identification [8].

Currently, parameter identification methods mainly include offline identification and online identification [9]. Offline identification estimates motor parameters by applying specific voltage or current excitation signals while the motor is stationary or before no-load startup. Such methods are executed only once before motor startup or during maintenance; therefore, they cannot track parameter changes during operation, such as resistance variation caused by temperature rise, inductance nonlinearity due to magnetic circuit saturation, or flux linkage attenuation caused by permanent magnet demagnetization. Online identification refers to a class of methods that continuously update motor parameters during normal motor operation using real-time collected electrical signals. The most widely used online identification methods include the least squares method [10, 11], extended Kalman filter [12], model reference adaptive system [13, 14], as well as optimization algorithms [15, 16] and neural network algorithms [17]. Among these approaches, optimization algorithms solve complex problems by mimicking the collective behavior and information-sharing mechanisms of biological populations [18]. They have been widely applied in optimization, machine learning, data mining, and intelligent control. In the field of PMSM identification, swarm intelligence algorithms have demonstrated excellent application value [19]. An online particle swarm optimization (PSO)-based identification method was proposed in [20]. Although it successfully identified motor parameters, only two parameters could be estimated simultaneously because of model rank deficiency. In contrast, another PSO algorithm was proposed in [21], which could accurately identify the four parameters (R_s, L_d, L_q, ψ_f) of the PMSM, but it did not verify whether the results of multiple runs converged consistently. An improved coati optimization algorithm was proposed in [22]. However, the nonlinear effects introduced by the VSI were not considered, leaving room for further improvement in identification accuracy.

Currently, one of the main factors affecting the identification accuracy and stability of optimization algorithms is inverter nonlinearity. The inverter dead-time effect distorts the sampled terminal signals and introduces significant harmonic components. If the collected voltage is directly used for identification, systematic bias is introduced [23]. To compensate for inverter-induced identification errors, a dead-time compensation-based identification method was proposed in [24]. In this method, the dead time is directly added to the inverter, after which the motor parameters are accurately identified using a particle swarm algorithm. The results show that, under both steady-state and

* Corresponding author: Qianghui Xiao (1278341228@qq.com).

dynamic conditions, this method achieved more accurate parameter identification and faster identification speed than the uncompensated case. In contrast, the method proposed in [25] directly estimates the dead-time voltage to improve parameter-identification accuracy. However, due to model constraints, this method is only applicable to SPMSMs (Surface-Mounted Permanent Magnet Synchronous Motors). Most existing methods rely on accurate dead-time models to compensate for nonlinear effects, which are not suitable for various operating conditions [26].

Black-winged Kite Algorithm (BKA) is a recently developed swarm intelligence optimization method derived from the predatory behaviors of black-winged kites observed in nature [27]. By simulating hovering, patrolling, attacking, and migration behaviors, BKA can efficiently solve complex optimization problems. The results reported in [28] indicate that the improved BKA performs well for multiple complex engineering design problems. The unmanned aerial vehicle (UAV) path-planning problem was addressed using an improved black-winged kite algorithm integrated with chaotic mapping and Gaussian mutation techniques [29]. In [30], BKA was combined with a machine-learning prediction model, demonstrating its strong generalization capability.

Although various BKA variants have been proposed by integrating different enhancement strategies, these methods are mainly designed for general numerical optimization problems. Their improvements are generally problem-independent and do not explicitly consider the characteristics of PMSM parameter identification, such as multimodal objective functions and the need for stable convergence with repeated identification tasks. Therefore, directly applying existing improved BKA to PMSM parameter identification may not fully exploit their optimization potential.

To improve the parameter-identification accuracy and convergence performance of PMSMs, this study proposes a BKA-based identification method with compensation for inverter nonlinearity. The primary contributions of this work are summarized as follows:

1) A 5th- and 7th-order harmonic voltage compensation strategy was proposed to suppress the influence of inverter nonlinearity on PMSM parameter identification. The proposed method does not require an explicit inverter model, offering improved identification performance with broad applicability.

2) The Good Point Set (GPS) initialization strategy was incorporated into the BKA to generate a more uniformly distributed initial population. Considering the significant differences in the magnitudes of PMSM parameters, this strategy improved the coverage of the search space and reduced the risk of premature convergence caused by uneven initial population distribution.

3) A Thinking Innovation Strategy was incorporated into the attack phase of the black-winged kite to enrich the search trajectories and enhance the balance between exploration and exploitation, thereby improving the convergence efficiency of the algorithm.

Experimental results demonstrate that, under VSI nonlinearity, the proposed method achieves higher identification accuracy and faster convergence under steady-state conditions, particularly in the low-speed operating region.

2. MATHEMATICAL MODEL OF PMSM AND PARAMETER IDENTIFICATION MODEL

2.1. Mathematical Model of PMSM

In the d-q axis coordinate system, the voltage equations for an ideal PMSM can be expressed as follows:

$$\begin{cases} u_d = R_s i_d + L_d \frac{di_d}{dt} - \omega_e L_q i_q \\ u_q = R_s i_q + L_q \frac{di_q}{dt} + \omega_e L_d i_d + \omega_e \psi_f \end{cases} \tag{1}$$

where u_d, u_q, i_d, and i_q denote the d-q axis stator voltages and stator currents, respectively; R_s, ω_e, L_d, and L_q denote the stator resistance, electrical angular velocity, d-axis stator inductance, and q-axis stator inductance, respectively; ψ_f is the permanent magnet flux linkage.

For conventional vector control, the $i_d = 0$ control strategy is generally adopted to reduce motor losses and improve the system power factor. The mathematical equations of the PMSM under vector control are as follows:

$$\begin{cases} u_d = R_s i_d - \omega_e L_q i_q \\ u_q = R_s i_q + \omega_e L_d i_d + \omega_e \psi_f \end{cases} \tag{2}$$

Equation (2) represents an underdetermined system containing four parameters (R_s, L_d, L_q, ψ_f) with a rank of two. Consequently, this system possesses an infinite number of solutions, making it impossible to identify the four parameters uniquely.

2.2. Parameter Identification Model

To construct a fully determined system, an alternating control mode between $i_d = 0$ and $i_d = -2$ is adopted. As shown in Fig. 1, this is implemented by periodically injecting a negative step current of $i_d = -2$ into the d-axis. Parameter identification for a single cycle is achieved by transmitting the collected data to the intelligent optimization algorithm, and the duration of data acquisition can be adjusted according to different requirements. For parameter identification, the data collected during each cycle are transmitted to the host computer, where the optimization algorithm is executed.

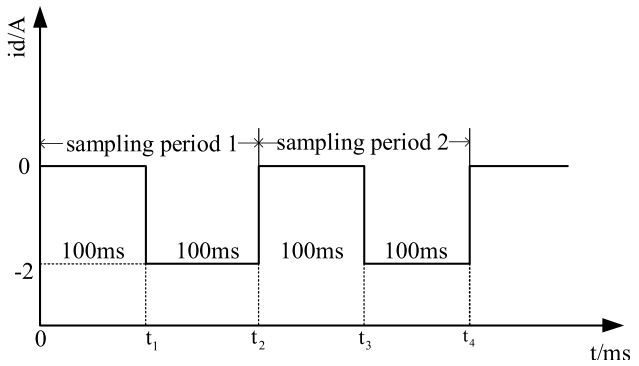

FIGURE 1. Sampling period diagram.

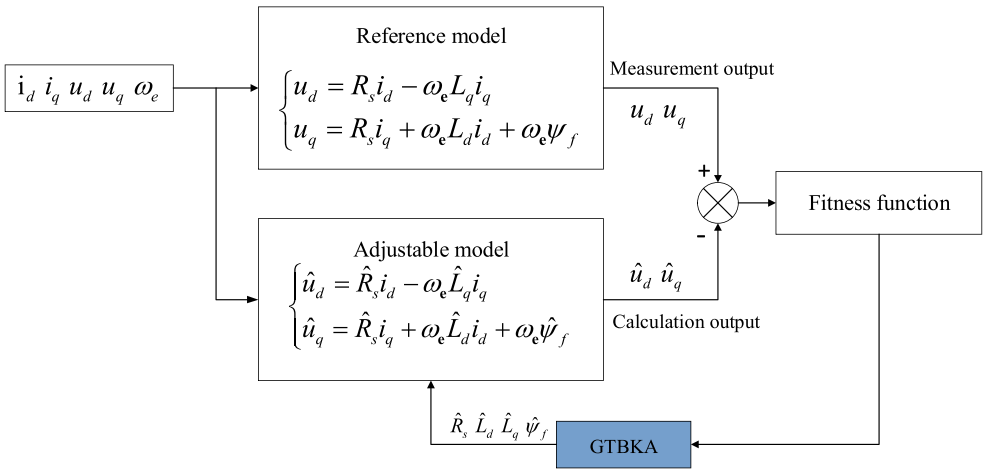

FIGURE 2. Schematic diagram of parameter identification.

By collecting an equal number of data points under both the $i_d = 0$ and $i_d = -2$ operating states, a fourth-order fully-determined discrete system of equations can be obtained as follows:

$$\begin{cases} u_{d0}(k) = -\omega_{e0}(k) L_q i_{q0}(k) \\ u_{q0}(k) = R_s i_{q0}(k) + \omega_{e0}(k) \psi_f \\ u_{d1}(k) = R_s i_{d1}(k) - \omega_{e1}(k) L_q i_{q1}(k) \\ u_{q1}(k) = R_s i_{q1}(k) + \omega_{e1}(k) (L_d i_{d1}(k) + \psi_f) \end{cases} \tag{3}$$

Data with the subscript "0" are collected under the control strategy with $i_d = 0$, while data with the subscript "1" are obtained under the control strategy with $i_d = 2$. The terms $u_{d0}(k)$, $u_{q0}(k)$, $i_{q0}(k)$, and $\omega_{e0}(k)$ represent the k-th sampled data during the 0-t_1 period, whereas $u_{d1}(k)$, $u_{q1}(k)$, $i_{q1}(k)$, and $\omega_{e1}(k)$ represent the k-th sampled data during the t_1-t_2 periods.

Based on the motor model, the mathematical model of the adjustable model is as follows:

$$\begin{cases} \hat{u}_{d0}(k) = -\omega_{e0}(k) \hat{L}_q i_{q0}(k) \\ \hat{u}_{q0}(k) = \hat{R}_s i_{q0}(k) + \omega_{e0}(k) \hat{\psi}_f \\ \hat{u}_{d1}(k) = \hat{R}_s i_{d1}(k) - \omega_{e1}(k) L_q i_{q1}(k) \\ \hat{u}_{q1}(k) = \hat{R}_s i_{q1}(k) + \omega_{e1}(k) \left(\hat{L}_d i_{d1}(k) + \hat{\psi}_f\right) \end{cases} \tag{4}$$

In the adjustable model, the d-axis and q-axis stator voltages are denoted as $\hat{u}_{d0}(k)$, $\hat{u}_{q0}(k)$, $\hat{u}_{d1}(k)$, and $\hat{u}_{q1}(k)$; the stator resistance is denoted as $\hat{R}_s$; the d-axis and q-axis stator inductances are denoted as $\hat{L}_d$ and $\hat{L}_q$; the permanent magnet flux linkage is denoted as $\hat{\psi}_f$.

In the PMSM vector control system, the fitness function can be formulated as follows:

$$Fitness = (u_{d0} - \hat{u}_{d0})^2 + (u_{q1} - \hat{u}_{q1})^2 \tag{5}$$

The inputs to both the reference and adjustable model are $u_d, u_q, i_d, i_q, \omega_e$, and u_d and u_q are also the outputs. A fitness function was employed to evaluate the difference between the outputs of the two models. The principle of parameter identification is illustrated in Fig. 2. The Good-point-set and Thinking-enhanced Black-winged Kite Algorithm (GTBKA) minimizes the fitness function by continuously updating the parameters of the adjustable model. The iterative process continues until the stopping criterion is satisfied. The resistance, inductance, and flux linkage obtained at this stage can be regarded as the identified parameter values of the system.

Figure 3 presents a flowchart of the PMSM parameter identification process. The entire procedure, from the acquisition of electrical signals to the output of the identification results, is illustrated.

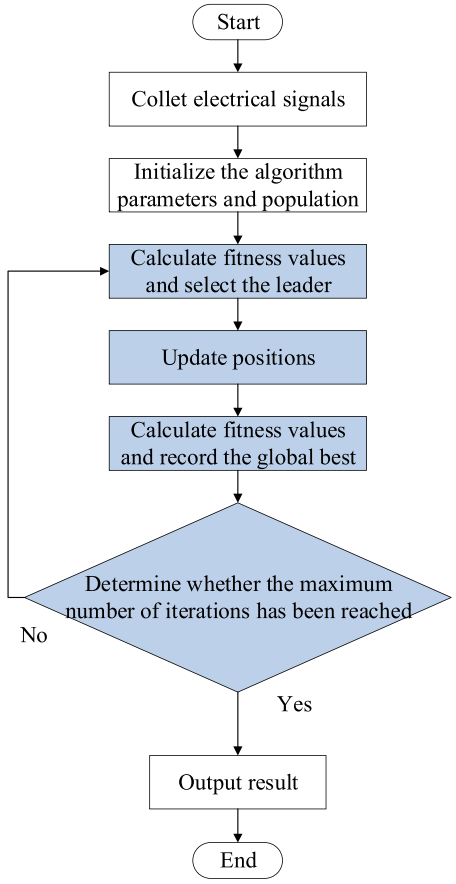

FIGURE 3. Flowchart of the parameter identification process.

FIGURE 4. Diagram of the harmonic current conversion module.

3. 5TH AND 7TH HARMONIC COMPENSATION

The nonlinearity of the VSI introduces significant harmonic components into the PMSM current, particularly the 5th- and 7th-order harmonics. Because the parameter-identification model is established under ideal inverter conditions, harmonic disturbances degrade the quality of the collected signals used for identification. Consequently, both the estimation accuracy and convergence stability of the algorithm are adversely affected. To suppress the impact of VSI nonlinearity on the identification process, this study proposes a compensation approach based on the injection of 5th- and 7th-order harmonic components. Consequently, both the accuracy and stability of the parameter identification were effectively improved.

The steady-state voltage equation of the 5th harmonic in the *dq*-axis is given as follows:

$$\begin{cases} u_{d5\text{th}} = 5\omega L_q i_{q5\text{th}} + R_s i_{d5\text{th}} \\ u_{q5\text{th}} = -5\omega L_d i_{d5\text{th}} + R_s i_{q5\text{th}} \end{cases} \tag{6}$$

where $u_{d5\text{th}}$ and $u_{q5\text{th}}$ are the 5th harmonic voltage on the d-axis and q-axis, respectively. Similarly, $i_{d5\text{th}}$ and $i_{q5\text{th}}$ are the 5th harmonic currents on the d-axis and q-axis, respectively.

The steady-state voltage equation of the 7th harmonic in the *dq*-axis is as follows:

$$\begin{cases} u_{d7\text{th}} = -7\omega L_q i_{q7\text{th}} + R_s i_{d7\text{th}} \\ u_{q7\text{th}} = 7\omega L_d i_{d7\text{th}} + R_s i_{q7\text{th}} \end{cases} \tag{7}$$

where $u_{d7\text{th}}$ and $u_{q7\text{th}}$ are the 7th harmonic voltage on the d-axis and q-axis, respectively. Similarly, $i_{d7\text{th}}$ and $i_{q7\text{th}}$ are the amplitudes of the 7th harmonic current on the d-axis and q-axis, respectively.

As shown in Fig. 4, the 5th and 7th harmonics are extracted from the three-phase currents using the harmonic voltage compensation module. Through calculations based on the steady-state equations of the harmonic voltages, $u_{d5\text{th}}$, $u_{q5\text{th}}$, $u_{d7\text{th}}$, and $u_{q7\text{th}}$ are obtained.

The compensation voltage is given as:

$$\begin{cases} u_{\alpha\_com} = u_{\alpha 5\text{th}} + u_{\alpha 7\text{th}} \\ u_{\beta\_com} = u_{\beta 5\text{th}} + u_{\beta 7\text{th}} \end{cases} \tag{8}$$

The compensation voltages u_{a_com} and u_{β_com} are respectively added to the voltage signals. By doing so, the random disturbances in the inputs of the algorithm are reduced, and the collected data are made closer to those of the ideal model.

4. GTBKA

4.1. BKA

The Black-winged Kite Algorithm (BKA) is an efficient and lightweight metaheuristic optimization technique established by mimicking the hunting strategies and migration patterns of black-winged kites in nature [27]. In the attack phase, different hunting strategies are employed to achieve global exploration in the search domain. The mathematical formulation describing this process is as follows:

$$y_{t+1}^{i,j} = \begin{cases} y_t^{i,j} + m\left(1 + \sin\left(rand\right)\right) \times y_t^{i,j} & g < rand \\ y_t^{i,j} + m \times \left(2rand - 1\right) \times y_t^{i,j} & else \end{cases} \tag{9}$$

$$m = 0.05 \times e^{-2\times\left(\frac{t}{T}\right)^2} \tag{10}$$

where $y_t^{i,j}$ and $y_{t+1}^{i,j}$ are the location of the ith individual in the jth dimension at iteration steps t and $t+1$, respectively; parameter *rand* denotes a uniformly distributed random variable in the interval [0, 1]; g is a fixed constant with a value of 0.9; T represents the maximum number of iterations; and t indicates the current iteration number.

In Eq. (9), the position-update behavior of the black-winged kite is modeled under two hunting scenarios: prey detection and dive attack. The parameter m represents the attack step size, which gradually decreases with the iteration number. This mechanism enables a smooth transition from global exploration to local exploitation. The search process alternates between random sinusoidal perturbation and random positive-negative perturbation. This mechanism helps balance exploration and exploitation throughout the optimization process.

Figure 5 illustrates the migration process of the black-winged kite population. If the fitness value of the current leader is lower than that of a randomly selected individual, it abandons its leadership role and rejoins the migrating population. This indicates

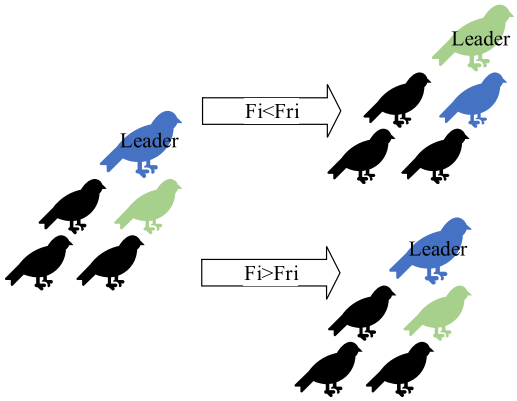

FIGURE 5. Migration phase of the black-winged kites.

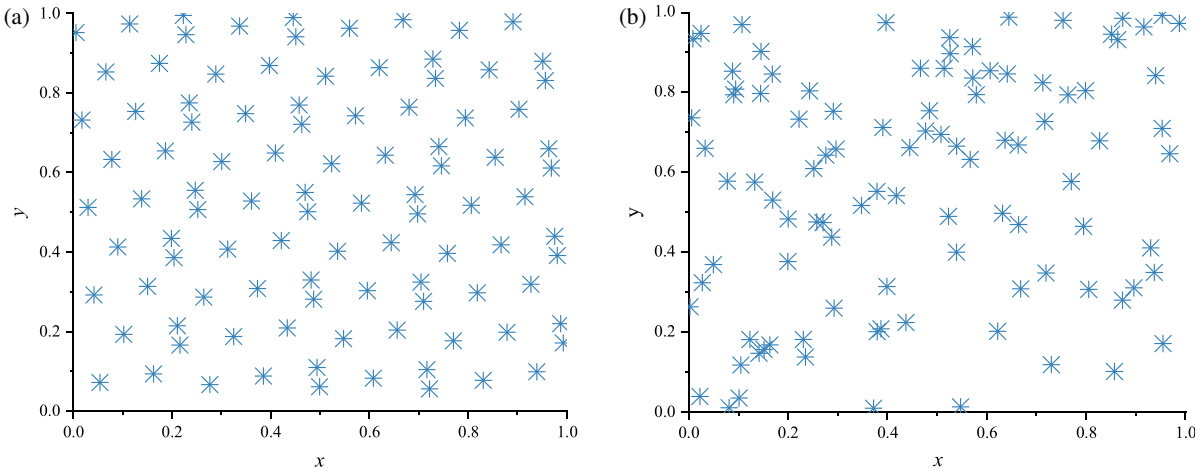

FIGURE 6. Comparison diagram of population distribution. (a) Good point set initialization and (b) random initialization.

that it can no longer effectively guide population evolution. In contrast, if the current leader exhibits a better fitness value than the randomly selected individual, it maintains its leadership status and continues guiding the population toward the target location. The migration behavior of the black-winged kite is mathematically formulated as follows:

$$y_{t+1}^{i,j} = \begin{cases} y_t^{i,j} + C(0,1) \times \left(y_t^{i,j} - L_t^j \right) & F_i < F_{ri} \\ y_t^{i,j} + C(0,1) \times \left(L_t^j - v \times y_t^{i,j} \right) & else \end{cases} \tag{11}$$

$$v = 2 \times \sin\left(rand + \pi/2\right) \tag{12}$$

where L_t^j represents the leader's location in dimension j at iteration t; $y_t^{i,j}$ and $y_{t+1}^{i,j}$ represent the positions of the ith individual in the jth dimension at iteration t and $t+1$, respectively; F_i is the fitness value of the black-winged kite's current position at iteration t; F_{ri} represents the fitness value of a randomly selected location within the same dimension and iteration; $C(0,1)$ denotes the Cauchy mutation. When $\delta = 1$ and $\mu = 0$, its probability density function becomes the standard form, expressed as:

$$f(x, \delta, \mu) = \frac{1}{\pi} \frac{1}{x^2 + 1}, \quad -\infty < x < \infty \tag{13}$$

4.2. Good Point Set

The Good Point Set (GPS) is a number-theory-based technique used to enhance the initialization distribution of population individuals. By employing specific mathematical construction rules, GPS generates uniformly distributed sample points across the search space. This improves the search capability, solution accuracy, and algorithm stability. Let G_s be the unit cube in the s-dimensional Euclidean space. The set $P_n(k)$ is defined as:

$$P_n(k) = \left(\left\{ q_1^{(n)} \cdot k \right\}, \left\{ q_2^{(n)} \cdot k \right\}, \ldots, \left\{ q_s^{(n)} \cdot k \right\} \right), \quad 1 \le k \le s \tag{14}$$

The deviation of this point set satisfies $\varphi(n) = C(r,\varepsilon) n^{-1+\varepsilon}$, where $C(r,\varepsilon)$ is a constant that depends only on r and ε (with $\varepsilon > 0$). Then, $P_n(k)$ is called a good point set.

$$r_i = 2\cos\frac{2\pi i}{p}, \quad 1 \le i \le s \tag{15}$$

where p is the smallest prime number that satisfies the condition $(p-3)/2 \ge s$.

The redefined strategy for initial population generation in the BKA is defined as follows:

$$X_i = (BK_{ub} - BK_{lb}) \cdot \left\{ r_j^{(i)} \cdot k \right\} + BK_{lb} \tag{16}$$

where BK_{lb} and BK_{ub} represent the lower and upper boundary values of the jth dimension corresponding to the ith black-winged kite, respectively.

Figure 6 presents a comparison of the population distributions in a two-dimensional search domain obtained using the GPS initialization method and the traditional random initialization approach. The BKA conventionally initialized population exhibits obvious aggregation in certain areas, leading to an uneven spatial distribution. By contrast, the population generated using the GPS method is dispersed more uniformly across the entire search space. As a result, the diversity of the initial population is significantly improved, which helped prevent the algorithm from prematurely converging to local optima caused by insufficient population diversity. Random initialization often leads to large variations in optimization results across repeated runs. In contrast, the GPS-based approach provides a stable and consistent initial population for each run, thereby improving the stability and accuracy of parameter identification.

4.3. Thinking Innovation Strategy

In the early stage of optimization, BKA exhibits strong global search capability and rapidly explores the search space. However, individuals rapidly converge toward the current best solution, reducing population diversity and increasing the risk of premature convergence to local optima. Consequently, the accuracy and stability of parameter identification are degraded.

To address the issues, a Thinking Innovation Strategy (TIS) mechanism is designed in the attack phase of BKA in this study. Through an innovative update mechanism guided by superior individuals, the search capability is enhanced, and the ability of the algorithm to escape from local optima is improved [31].

In the attack phase of the black-winged kite, hovering behavior is primarily employed for global exploration to search for and attack prey. During this process, the entire search region is explored, and hovering is performed near areas where prey is more likely to appear, namely around the current best position. This strategy assumes that the black-winged kite imitates human innovative thinking during the hunting process. Human problem solving generally relies on two categories of accumulated knowledge and experience. One category is initially relied upon by the brain, whereas the other is gradually accumulated through personal experience.

The expression of Depth of Knowledge (DOK) is given as follows:

$$DOK1 = Z + \left(\frac{t}{T}\right)^{0.5} \tag{17}$$

$$DOK2 = t^{10} \tag{18}$$

$$DOK = DOK1 + DOK2 \tag{19}$$

DOK1 represents knowledge and experience accumulated over time; *DOK2* represents continuous acquisition and storage of information; Z is a constant with a value of 0.5; t denotes the current number of iterations; T denotes the maximum number of iterations.

In addition to accumulated knowledge and experience, humans solve problems through imagination, namely the ability to generate new solutions by reorganizing perceptual information in innovative ways. During the innovation phase, the position of the black-winged kite is mainly updated according to the variations of previously identified superior individuals. Imagination (IM) can be understood as the capacity to form novel images through the creative recombination of perceptual materials. The expression of IM is given as follows:

$$IM = \pi \times L_t^j \times rand \tag{20}$$

where *IM* represents the innovation factor, which is used to generate adaptive nonlinear search directions through the tangent mapping.

The update formula of the GTBKA integrated with the Thinking Innovation Strategy during the hovering phase is as follows:

$$y_{t+1}^{i,j} = \begin{cases} y_t^{i,j} + m\left(1 + \sin\left(rand\right)\right) \times \left(\tan\left(IM - \frac{\pi}{2}\right) \right. \\ \left. + \left(\frac{y_t^{i,j}}{DOK} + L_t^j\right)\right) & g < rand \\ y_t^{i,j} + m\left(2rand - 1\right) \times \left(\tan\left(IM - \frac{\pi}{2}\right) \right. \\ \left. + \left(\frac{y_t^{i,j}}{DOK} + L_t^j\right)\right) & else \end{cases} \tag{21}$$

In the BKA, the attack phase primarily relies on an update mechanism based on proportional perturbation of the current position. In contrast, after the TIS is incorporated, the attack phase is enhanced. Nonlinear jumps are utilized to increase population diversity. Information from the leader is employed to improve search directionality. The search scale is dynamically adjusted through the DOK.

5. IDENTIFICATION WITH GTBKA

The flowchart of the GTBKA is shown in Fig. 7. In the population initialization stage, the good point set is adopted by the algorithm. In the attack stage, the TIS is designed for spatial search. The position update is then continued in the migration stage. Finally, the best individual position is output. Each dimension of the position corresponds to a PMSM parameter result.

6. EXPERIMENTAL RESULTS

To verify the effectiveness of the proposed approach, a hardware-in-the-loop simulation platform for PMSM was established based on the RT-LAB real-time simulator. The control algorithm is implemented using a TMS320F2812 DSP controller. The configuration of the RT-LAB experimental platform is illustrated in Fig. 8 and Fig. 9. During the experiment, the collected data were transmitted to the host computer, where the proposed algorithm was executed to accomplish parameter identification.

In this experiment, six algorithms are selected for comparative evaluation. For algorithms marked with the subscript "com", harmonic compensation is adopted. GBKA (Good-point-set-based Black-winged Kite Algorithm) is an improved version of the BKA algorithm. Its initialization is carried out using the GPS. The search ranges for PSO, WOA (Whale Optimization Algorithm), BKA, BKA_com, GBKA_com, and GTBKA_com are set identically. The number of iterations is fixed at 200. To ensure that each algorithm is able to converge to a solution within the same iteration count most of the time, for PSO and WOA (Whale Optimization Algorithm) [32], the population size is set to 200, and for BKA, BKA_com, GBKA_com, and GTBKA_com, the population size is set to 50. To ensure statistical reliability and reduce the influence of randomness, each algorithm is independently executed 30 times. The reported average values, as well as the corresponding maximum and minimum errors, are calculated from these 30 independent runs.

The PMSM vector control system model is executed in RT-LAB, and the vector control system is shown in Fig. 10. The PMSM parameters are shown in Table 1.

TABLE 1. The parameters of PMSM.

Parameter	Value	Parameter	Value
Pole Pairs	4	ψ_f (Wb)	0.08
R_s (Ω)	0.29	Rated Torque (N·m)	50
L_d (mH)	0.206	Rated Speed (rpm)	3000
L_q (mH)	0.550	Rated Power (kW)	1.0

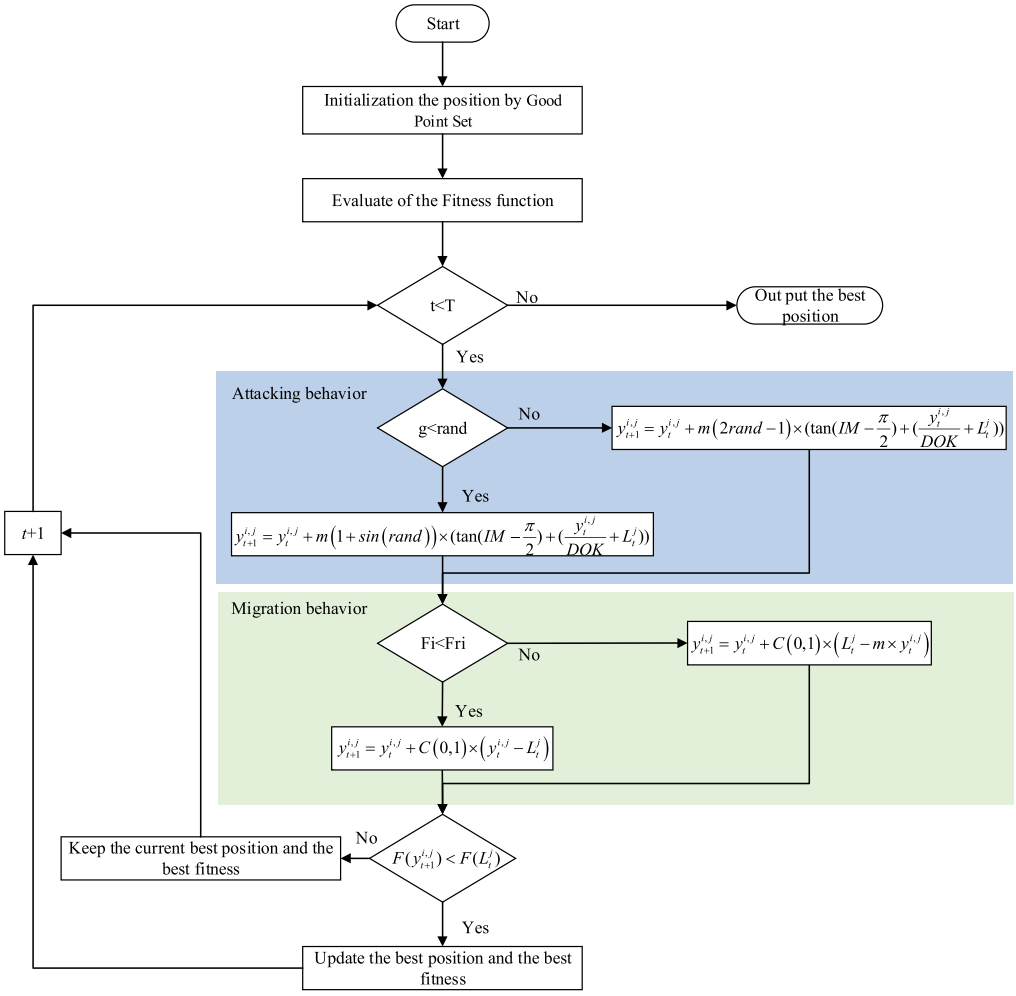

FIGURE 7. The flowchart of GTBKA.

TABLE 2. R_s identification results in general situation.

Parameter	PSO	WOA	BKA	BKA_com	GBKA_com	GTBKA_com
Average R_s (Ω)	0.2203	0.2271	0.2699	0.3004	0.2998	0.2983
Maximum Error (%)	30.7652	256142	85139	5.5993	43846	2.8807
Minimum Error (%)	22.1586	153910	50405	3.0658	30397	28806

TABLE 3. L_d identification results in general situation.

Parameter	PSO	WOA	BKA	BKA_com	GBKA_com	GTBKA_com
Average L_d (mH)	0.1587	0.1836	0.1936	0.1988	0.2121	0.211
Maximum Error (%)	28.3889	17.6843	133327	4.7464	4.8208	24788
Minimum Error (%)	20.0575	6.8264	36441	24797	26081	24744

6.1. General Situation

The results in Tables 2–5 indicate that the original BKA is more suitable for PMSM parameter identification than PSO and WOA. However, its identification accuracy remains inferior to that of the improved algorithms. Specifically, the maximum error for Ld reaches 13.3327%, and a large fluctuation range is also observed. This phenomenon is mainly attributed to the modeling errors introduced by VSI nonlinearity. After harmonic compensation, both the identification accuracy and stability of BKA_com are improved. With the incorporation of the Good Point Set strategy, the convergence accuracy, convergence speed, and stability are further enhanced. In particular, the minimum error of each parameter approaches the current optimum, although slight instability remains. By further

TABLE 4. L_q identification results in general situation.

Parameter	PSO	WOA	BKA	BKA_com	GBKA_com	GTBKA_com
Average L_q (mH)	0.5504	0.5505	0.5505	0.5503	0.5501	0.5500
Maximum Error (%)	0.5948	0.9043	0.1289	0.0997	0.0255	0.0049
Minimum Error (%)	0.0809	0.0925	0.394	0.047	0.047	0.047

TABLE 5. ψ_f identification results in general situation.

Parameter	PSO	WOA	BKA	BKA_com	GBKA_com	GTBKA_com
Average ψ_f (Wb)	0.0858	0.0852	0.0817	0.0792	0.0793	0.0793
Maximum Error (%)	10.9811	149336	25974	15575	12954	0.8390
Minimum Error (%)	1.5284	3.3100	13769	0.8275	0.8504	0.8371

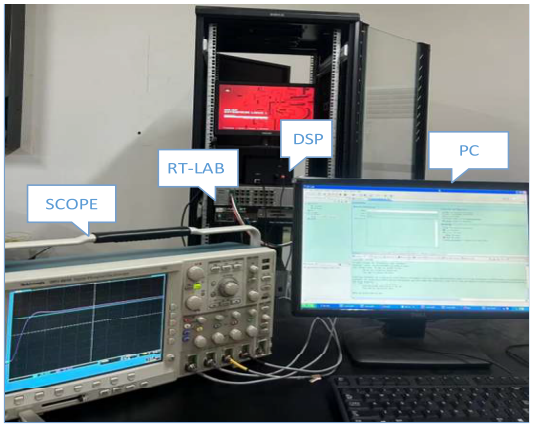

FIGURE 8. Experimental equipment.

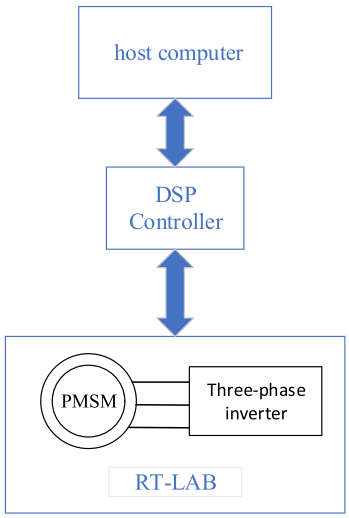

FIGURE 9. RT-LAB experimental platform.

incorporating the Thinking Innovation Strategy, GTBKA_com achieves the highest identification accuracy among the four algorithms. The average identification results of GTBKA_com are 0.2983 Ω for R_s, 0.2110 mH for L_d, and 0.0793 Wb for ψ_f, with the highest accuracy attained for L_q. Moreover, the results obtained from multiple independent runs are nearly identical, and the difference between the maximum and minimum errors is controlled within 0.01%. Therefore, GTBKA_com provides an effective solution for high-precision online PMSM parameter identification, particularly in applications requiring both high accuracy and strong stability.

Figure 11 shows the iterative convergence curves of the motor parameters under general conditions.

Figure 11 illustrates the convergence curves of the motor parameters under general conditions. Among all the compared algorithms, GTBKA_com achieves the highest identification accuracy and the fastest convergence speed, with almost no fluctuations observed during the later iterations. By contrast, PSO and WOA exhibit relatively poor convergence performance. Both algorithms tend to become trapped in local optima during the early stages of the search process, making it difficult to further approach the global optimum. The BKA exhibits limited capability in escaping from local optima during the identification process, which slows down convergence and results in unstable identification outcomes. After harmonic compensation is introduced, the parameter identification accuracy is significantly improved, and convergence stability is enhanced, especially for R_s. However, the inherent shortcomings of the algorithm are only partially alleviated and still present. Compared with BKA_com, GBKA_com adopts the Good Point Set as a fixed and uniform initialization strategy, enabling the algorithm to rapidly converge toward the vicinity of the reference values while reducing fluctuations in the identification results. After incorporating the Thinking Innovation Strategy, the advantages of the Good Point Set are retained, while the identification accuracy is further improved, enabling the algorithm to converge within approximately 50 iterations. More importantly, the identification results become considerably more stable, and the algorithm is less likely to converge erroneously during the later stages of iteration.

Table 6 shows that the execution time of GTBKA is 0.0535 s, which is only slightly higher than that of BKA due to the additional search strategies. GTBKA remains considerably faster than PSO and WOA. Considering that PMSM parameters vary much more slowly than the sampling period, the running time of the algorithm is also shorter than the sampling period. Therefore, the execution time of 0.0535 s indicates that the proposed

TABLE 6. Execution time.

Algorithm	PSO	WOA	BKA	BKA_com	GBKA_com	GTBKA_com
Running time	0.1536 s	0.1076 s	0.0425 s	0.0400 s	0.0427 s	0.0535 s

TABLE 7. R_s identification results in low-speed situation.

Parameter	PSO	WOA	BKA	BKA_com	GBKA_com	GTBKA_com
Average R_s (Ω)	0.2087	0.3795	0.2870	0.2844	0.2850	0.2907
Maximum Error (%)	48.1614	34.9990	156573	37326	36934	0.2456
Minimum Error (%)	10.2629	26.5370	0.9409	18435	0.3502	0.2387

TABLE 8. L_d identification results in low-speed situation.

Parameter	PSO	WOA	BKA	BKA_com	GBKA_com	GTBKA_com
Average L_d (mH)	0.3280	0.2677	0.1525	0.1935	0.1948	0.1980
Maximum Error (%)	63.8660	50.4671	325379	71861	58220	3.9023
Minimum Error (%)	37.1851	11.6266	257328	30194	39749	3.8412

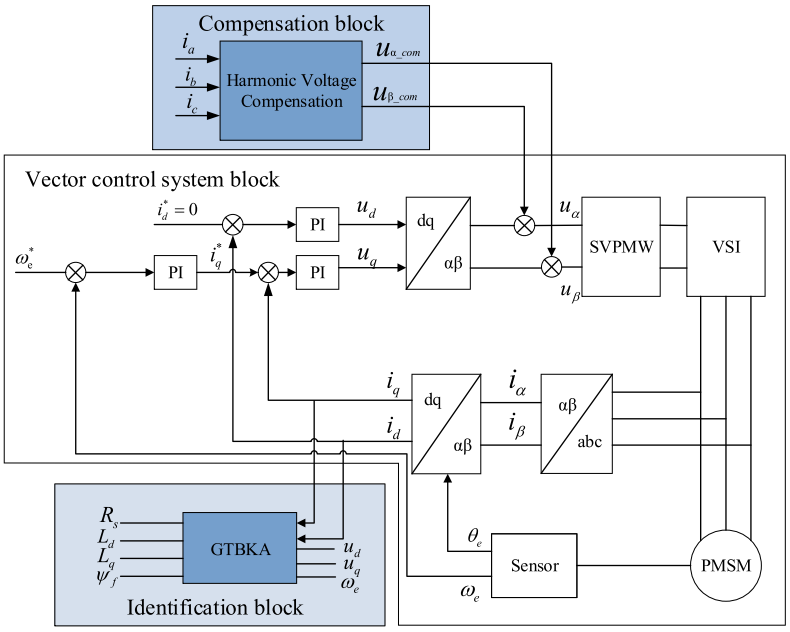

FIGURE 10. Model of the PMSM vector control system.

GTBKA possesses preliminary real-time capability for online parameter identification under the investigated steady-state operating conditions.

6.2. Low-Speed Situation

When the motor operates in the low-speed region, the back electromotive force becomes weak, thereby reducing the accuracy of parameter identification. In addition, the influence of VSI nonlinearity becomes more pronounced, resulting in larger identification errors. To validate the identification performance of the proposed algorithm in the low-speed region, the algorithm was executed for identification at a motor speed of 300 r/min. The identification results of the compared algorithms are presented in Tables 7–10, and the convergence curves for each parameter are shown in Fig. 12.

Under low-speed operating conditions, PSO and WOA exhibit relatively poor parameter identification performance. For R_s and L_d, the maximum errors of PSO reach 48.1614% and 63.8660%, respectively, while those of WOA reach 34.9990% and 50.4671%, indicating that both algorithms are highly susceptible to the weakened back electromotive force and inverter

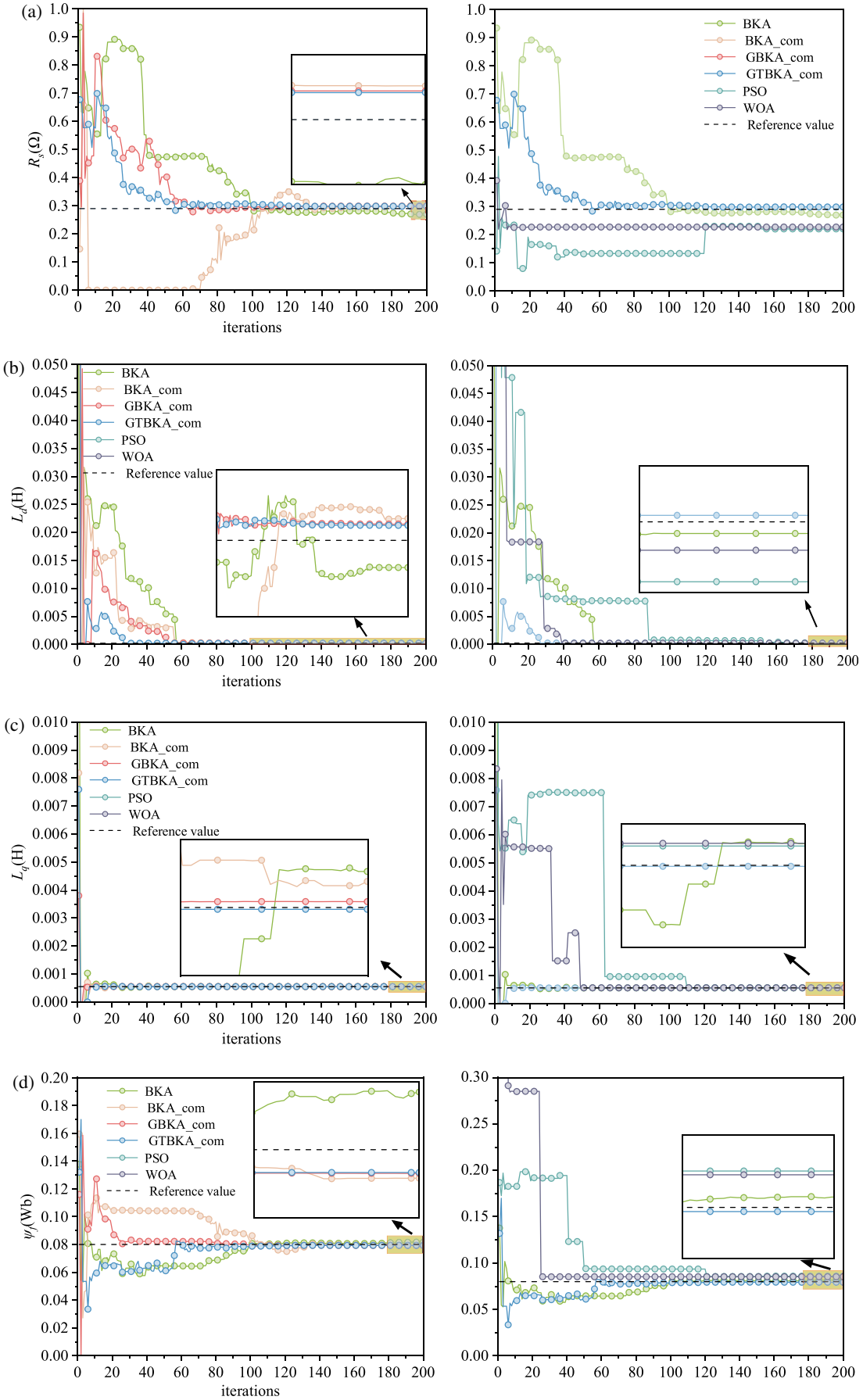

FIGURE 11. Convergence curves of the parameters under general conditions. (a) R_s convergence process, (b) L_d convergence process, (c) L_q convergence process, and (d) ψ_f convergence process.

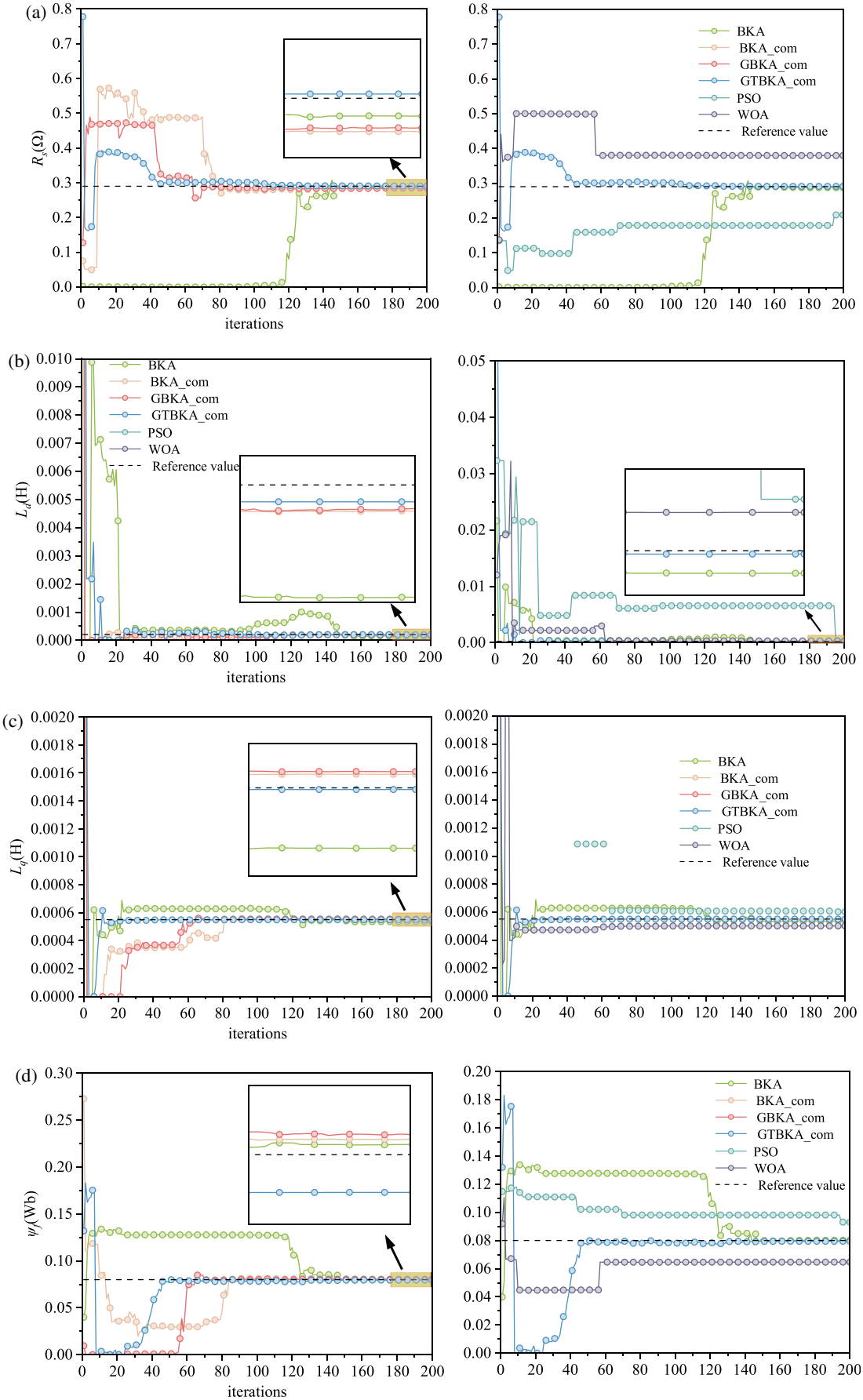

FIGURE 12. Convergence curves of the parameters under low-speed conditions. (a) R_s convergence process, (b) L_d convergence process, (c) L_{qs} convergence process, and (d) ψ_f convergence process.

TABLE 9. L_q identification results in low-speed situation.

Parameter	PSO	WOA	BKA	BKA_com	GBKA_com	GTBKA_com
Average L_q (mH)	0.5718	0.5008	0.5363	0.5530	0.5536	0.5500
Maximum Error (%)	8.9384	15.4340	28615	0.9819	10591	0.674
Minimum Error (%)	0.6797	7.2596	0.8180	0.4577	0.662	0.638

TABLE 10. ψ_f identification results in low-speed situation.

Parameter	PSO	WOA	BKA	BKA_com	GBKA_com	GTBKA_com
Average ψ_f (Wb)	0.0930	0.646	0.0802	0.808	0.805	0.795
Maximum Error (%)	194928	35.4958	16866	13075	0.7583	0.6945
Minimum Error (%)	5.7835	12.5900	0.2763	0.6724	0.6570	0.6511

nonlinearity in the low-speed region. Although acceptable identification accuracy can occasionally be achieved in individual runs, the large differences between the maximum and minimum errors demonstrate insufficient convergence stability.

Compared with PSO and WOA, the BKA achieved improved identification performance under low-speed operating conditions. However, the identification errors of the inductance parameters remained relatively large. In particular, for L_q, the maximum error reaches 32.5379%, and the minimum error is 25.7328%, indicating poor consistency in overall parameter identification. This phenomenon is mainly attributed to the weak back electromotive force in the low-speed region, which reduces the identifiability of the inductance parameters. Moreover, the weakened back electromotive force becomes more susceptible to the influence of the dead-time effect. After the 5th- and 7th-order harmonic compensation is introduced, the difference between the maximum and minimum errors of BKA_com can be controlled within 5%. Specifically, the maximum error of L_d is reduced to 7.1861%, and that of L_q is reduced to 0.9819%. The error of each parameter can be controlled within 8%. These results indicate that the proposed 5th- and 7th-order harmonic compensation method significantly improves the identification performance of L_d and L_q in the low-speed region, while the identification capability of the algorithm is further enhanced after harmonic compensation. With GTBKA_com, the identification results obtained from multiple runs converge to nearly identical values, and the difference between the maximum and minimum errors of ψ_f is only 0.0434%. Moreover, among all the algorithms, GTBKA_com yields the most accurate convergence results except for ψ_f.

Analysis of the six convergence curves shows that PSO and WOA exhibit relatively weak search capability under low-speed operating conditions. Under low-speed conditions, BKA is also highly susceptible to inverter dead-time effects, resulting in slow convergence and increased tendency to become trapped in local optima. After the introduction of 5th- and 7th-order harmonic compensation, the stability of parameter identification is significantly improved, while the number of iterations required for convergence is reduced. By further incorporating the proposed strategy, both the global search capability and the parameter convergence performance of the algorithm are further enhanced. GTBKA_com converges rapidly and stabilizes near the reference values within approximately 50 iterations, exhibiting the smallest fluctuations throughout the convergence process. These results demonstrate that the proposed algorithm also exhibits superior parameter identification capability for PMSMs under low-speed operating conditions.

7. CONCLUSION

This study addresses the degradation of parameter-identification performance caused by VSI nonlinearities. To address this issue, an enhanced BKA with harmonic compensation is developed to identify the stator resistance, inductances, and flux linkage of PMSMs. Based on the theoretical derivations and experimental investigations conducted under different operating conditions, the following conclusions can be obtained:

(1) The proposed harmonic compensation method dynamically compensates the 5th- and 7th-order harmonics, thereby reducing the influence of VSI nonlinearities on the sampled signals.

(2) The Good Point Set initialization mechanism is incorporated into the algorithm to construct a uniformly distributed fixed initial population within the search domain. Experimental comparisons indicate that the proposed GBKA_com not only accelerates the convergence process but also further improves the accuracy and robustness of parameter identification.

(3) A Thinking Innovation Strategy is incorporated into the attack phase of BKA, enabling the optimization process to mimic human-like problem-solving behavior during hunting.

Experimental results demonstrate that, under the investigated steady-state operating conditions affected by VSI nonlinearity, particularly in the low-speed steady-state region, the proposed strategy can effectively suppress identification fluctuations while further improving convergence speed and identification accuracy. In future work, the proposed method will be extended to dynamic operating conditions and integrated with adaptive control strategies to validate its effectiveness in practical PMSM drive systems.

ACKNOWLEDGEMENT

This work was supported by the Scientific Research Fund of Hunan Provincial Education Department under Grant Number 24A0395.

REFERENCES

[1] Wang, Y., H. Yu, S. Niu, J. Gu, Y. Liu, F. Cheng, T. Xia, and W. Zhang, "Adaptive observer-based current constraint control for electric vehicle used PMSM," *Applied Energy*, Vol. 360, 122802, 2024.

[2] Wang, Z., T. W. Ching, S. Huang, H. Wang, and T. Xu, "Challenges faced by electric vehicle motors and their solutions," *IEEE Access*, Vol. 9, 5228–5249, 2021.

[3] Zhang, Y., P. Yang, C. Liu, S. Li, K. Cao, Z. Liu, and Z. Cheng, "Improved model predictive torque control for PMSM based on anti-stagnation particle swarm online parameter identification," *Progress In Electromagnetics Research B*, Vol. 114, 51–66, 2025.

[4] Brescia, E., P. R. Massenio, M. D. Nardo, G. L. Cascella, C. Gerada, and F. Cupertino, "Nonintrusive parameter identification of IoT-embedded isotropic PMSM drives," *IEEE Journal of Emerging and Selected Topics in Power Electronics*, Vol. 11, No. 5, 5195–5207, 2023.

[5] Zhang, X., C. Zhang, Z. Wang, and J. Rodríguez, "Motor-parameter-free model predictive current control for PMSM drives," *IEEE Transactions on Industrial Electronics*, Vol. 71, No. 6, 5443–5452, 2024.

[6] Liu, Z., Y. Han, G. Feng, and N. C. Kar, "Efficient nonlinear multi-parameter decoupled estimation of PMSM drives based on multi-state voltage and torque measurements," *IEEE Transactions on Energy Conversion*, Vol. 38, No. 1, 321–331, 2023.

[7] Zwerger, T. and P. Mercorelli, "Backward extended Kalman filter to estimate and adaptively control a PMSM in saturation conditions," *IEEE Journal of Emerging and Selected Topics in Industrial Electronics*, Vol. 5, No. 2, 462–474, 2024.

[8] Li, X. and R. Kennel, "General formulation of Kalman-filter-based online parameter identification methods for VSI-fed PMSM," *IEEE Transactions on Industrial Electronics*, Vol. 68, No. 4, 2856–2864, 2021.

[9] Lian, C., F. Xiao, J. Liu, and S. Gao, "Parameter and VSI nonlinearity hybrid estimation for PMSM drives based on recursive least square," *IEEE Transactions on Transportation Electrification*, Vol. 9, No. 2, 2195–2206, 2023.

[10] Zhang, H., P. Ran, and Z. Zhang, "PMSM sensorless control based on super-twisting algorithm sliding mode observer with the IAORLS parameter estimations," *Scientific Reports*, Vol. 15, No. 1, 22386, 2025.

[11] Yu, H., J. Wang, and Z. Xin, "Model predictive control for PMSM based on discrete space vector modulation with RLS parameter identification," *Energies*, Vol. 15, No. 11, 4041, 2022.

[12] Wang, Z., X. Liu, W. Wang, Y. Lv, B. Yuan, W. Li, Q. Li, S. Wang, Q. Chen, and Y. Zhang, "UKF-based parameter estimation and identification for permanent magnet synchronous motor," *Frontiers in Energy Research*, Vol. 10, 855649, 2022.

[13] Wang, L., S. Zhang, C. Zhang, and Y. Zhou, "An improved deadbeat predictive current control based on parameter identification for PMSM," *IEEE Transactions on Transportation Electrification*, Vol. 10, No. 2, 2740–2753, 2024.

[14] Liu, Z.-H., J. Nie, H.-L. Wei, L. Chen, X.-H. Li, and M.-Y. Lv, "Switched PI control based MRAS for sensorless control of PMSM drives using fuzzy-logic-controller," *IEEE Open Journal of Power Electronics*, Vol. 3, 368–381, 2022.

[15] Ahandani, M. A., J. Abbasfam, and H. Kharrati, "Parameter identification of permanent magnet synchronous motors using quasi-opposition-based particle swarm optimization and hybrid chaotic particle swarm optimization algorithms," *Applied Intelligence*, Vol. 52, No. 11, 13 082–13 096, Feb. 2022.

[16] Liu, Z.-H., H.-L. Wei, X.-H. Li, K. Liu, and Q.-C. Zhong, "Global identification of electrical and mechanical parameters in PMSM drive based on dynamic self-learning PSO," *IEEE Transactions on Power Electronics*, Vol. 33, No. 12, 10 858–10 871, 2018.

[17] Wang, L., J. Yang, and H. Hu, "Predictive control of PMSM without differential beat current based on ADALINE neural network parameter identification," in *International Conference on Smartrail, Traffic and Transportation Engineering*, 581–588, Springer, Singapore, 2025.

[18] Hashim, F. A. and A. G. Hussien, "Snake optimizer: A novel meta-heuristic optimization algorithm," *Knowledge-Based Systems*, Vol. 242, 108320, 2022.

[19] Mohammed, H., Z. Abdul, and Z. Hamad, "Enhancement of GWO for solving numerical functions and engineering problems," *Neural Computing and Applications*, Vol. 36, No. 7, 3405–3413, 2024.

[20] Xie, C., S. Zhang, X. Li, Y. Zhou, and Y. Dong, "Parameter identification for SPMSM with deadbeat predictive current control using online PSO," *IEEE Transactions on Transportation Electrification*, Vol. 10, No. 2, 4055–4064, 2024.

[21] Zhou, S., D. Wang, and Y. Li, "Parameter identification of permanent magnet synchronous motor based on modified-fuzzy particle swarm optimization," *Energy Reports*, Vol. 9, 873–879, 2023.

[22] Yang, X., J. Zhan, Y. Shen, P. Liu, L. Guo, and Z. Zhang, "Parameter identification for SPMSM based on a superior ROA," *IEEE Transactions on Power Electronics*, Vol. 40, No. 6, 7615–7627, 2025.

[23] Hao, X. and Y. Luo, "An SMC-ESO-based distortion voltage compensation strategy for PWM VSI of PMSM," *IEEE Journal of Emerging and Selected Topics in Power Electronics*, Vol. 10, No. 5, 5686–5697, 2022.

[24] Zhang, Y., M. Zhou, C. Zhang, A. Shen, and L. Bing, "Identification of PMSM parameters with time-error compensated based on contractile factor antipredator PSO," *IEEE Transactions on Transportation Electrification*, Vol. 10, No. 2, 4006–4017, 2024.

[25] Liu, Z.-H., H.-L. Wei, Q.-C. Zhong, K. Liu, and X.-H. Li, "GPU implementation of DPSO-RE algorithm for parameters identification of surface PMSM considering VSI nonlinearity," *IEEE Journal of Emerging and Selected Topics in Power Electronics*, Vol. 5, No. 3, 1334–1345, 2017.

[26] Wang, C. and A. Wang, "Research on parameter identification algorithm of permanent magnet synchronous motor considering dead time compensation," *Progress In Electromagnetics Research C*, Vol. 138, 205–218, 2023.

[27] Wang, J., W.-C. Wang, X.-X. Hu, L. Qiu, and H.-F. Zang, "Black-winged kite algorithm: A nature-inspired meta-heuristic for solving benchmark functions and engineering problems," *Artificial Intelligence Review*, Vol. 57, No. 4, 98, 2024.

[28] Mohapatra, S., D. Kaliyaperumal, and F. S. Gharehchopogh, "A revamped black winged kite algorithm with advanced strategies for engineering optimization," *Scientific Reports*, Vol. 15, No. 1, 17681, 2025.

[29] Wang, S., B. Xu, Y. Zheng, Y. Yue, and M. Xiong, "Path optimization strategy for unmanned aerial vehicles based on improved black winged kite optimization algorithm," *Biomimetics*, Vol. 10, No. 5, 310, 2025.

[30] Zhang, X., K. Wu, C. Zhang, X. Shao, H. Shen, A. A. Heidari, C. Chen, H. Chen, and Z. Gao, "An enhanced black-winged kite algorithm boosted machine learning prediction model for patients' waiting time," *Biomedical Signal Processing and Control*, Vol. 105, 107425, 2025.

[31] Jia, H., X. Zhou, and J. Zhang, "Thinking Innovation Strategy (TIS): A novel mechanism for metaheuristic algorithm design and evolutionary update," *Applied Soft Computing*, Vol. 175, 113071, 2025.

[32] Mirjalili, S. and A. Lewis, "The whale optimization algorithm," *Advances in Engineering Software*, Vol. 95, 51–67, May 2016.